Peer-reviewed version available at *Molecules* **2018**, *23*, 3270; doi:10.3390/molecules23123270

Experimental and theoretical study on the synergistic inhibition effect of yridine derivatives and sulfur-containing compounds on the corrosion of carbon steel in CO_2-saturated 3.5 wt.% NaCl solution

Junlei Tang[a], Yuxin Hu[a], Zhongzhi Hang[b], Hu Wang[c], Yuanqiang Zhu[a], Yuan Wang[a], Zhen Nie[d], Yingying Wang[a]*

a School of Chemistry and Chemical Engineering, Southwest Petroleum University, Chengdu 610500, China

b CNPC Engineering Technology Research Company Limited., No.40 Jintang Road. Tanggu Binhai New Area, Tianjin 300451, China

c School of Material Science and Engineering, Southwest Petroleum University, Chengdu 610500, China

d Research Institute of Petroleum Exploration and Development, CNPC, Beijing 100083, China

Tel./fax: plus 86 028 83037361 senty78@126.com

Abstract

The corrosion inhibition performance of pyridine derivatives (4-methylpyridine and its quaternary ammonium salts) and sulfur-containing compounds (thiourea and mercaptoethanol) with different molar ratios on carbon steel in CO_2-saturated 3.5 wt.% NaCl solution was investigated by weight loss, potentiodynamic polarization, electrochemical impedance spectroscopy and scanning electron microscopy. The synergistic corrosion inhibition mechanism of mixed inhibitors was elucidated by the theoretical calculation and simulation. The molecule of pyridine derivatives compound with larger volume has the priority to adsorb on the metal surface, while

Peer-reviewed version available at Molecules 2018, 23, 3270; doi:10.3390/molecules23123270

the molecules of sulfur-containing compounds with smaller volume fill in vacancies. A dense adsorption film would be formed when 4-PQ and sulfur-containing compounds are added at a proper mole ratio.

Keywords: Corrosion inhibitor; Synergistic effect; Electrochemical measurements; Theoretical calculation

1. Introduction

Carbon dioxide (CO_2) corrosion is a serious problem in oil and gas wells and pipelines causing unacceptable electrochemical corrosion of carbon steel, especially in oil and gas production and transmission [1–4]. Due to low-cost and convenient, the injection of inhibitors is an economical and effective method for corrosion protection [5,6]. In general, corrosion inhibitors for carbon steel used in oilfield industry are organic compounds contain unsaturated bond or atoms such as N, O, S, etc. They can form coordination bonds with empty orbits of metal elements, and adsorb on the metal surface to protect metal material [7–9].

The corrosion inhibitor of single compound is often insufficient to protect carbon steel tubing and casing for oil production because of severe corrosive environment. The development of inhibitors mixture with a synergistic inhibition effect is the economical and effective way for increasing the inhibition efficiency, decreasing the amount of usage and diversifying the application of inhibitors in aggressive medium [10]. Many researchers have noticed the synergistic effects among specific substances, between organic and inorganic compounds [11–13], surfactants [14,15], or two organics [16,17]. However, the synergistic mechanism of organic compounds is complex, which highly depend on the compound structure. Pyridine and its

Peer-reviewed version available at *Molecules* **2018**, *23*, 3270; doi:10.3390/molecules23123270

derivatives as one of the important classes of pharmacological compound are widely used in medical industry and some literatures revealed pyridine derivatives were used as corrosion inhibitors having desirable effect in acid solutions. Researchers probed the special structure of those compounds to bridge between the experimental results and theoretical studies by quantum chemical studies [18–20]. Their corrosion inhibition effect could be owing to the heterocyclic structure with nitrogen atom [21–23]. However, it has rarely been studied in CO_2 environment. In another hand, sulfur compounds such like thiourea and mercaptoethanol have the protective effect for carbon steel determined by concentration and corrosion medium [24–26]. However, the dosage cost limit its further application. It is able to design economical and effective corrosion inhibitors mixtures if there is an efficient synergistic inhibition effect between pyridine derivatives and sulfur-containing compounds, which haven't been systematic investigated to the best of our knowledge.

More important, the classical adsorption model of mixed corrosion inhibitors which had the synergistic effect, considering the adsorption mechanism was that the inhibitor molecule with strong bonding preferentially adsorbed on the metal surface by the way of erect or tilted arrangement, and another inhibitor was superimposed on the void to form a coherent hydrophobic film as a barrier for migration of corrosive medium [27,28]. At present, although this typical theoretical model is widely accepted, the real adsorption configuration at the metal/solution interface is very difficult to be confirmed by the in-situ microscopic characterization in molecule-level. Many researchers have used molecular simulation methods to solve the issue of adsorption configuration, but a large number of reported simulations only used vacuum environment and many of them only simulated the adsorption behavior of a single molecule. The molecule dynamic simulations respect to the actual conditions

Peer-reviewed version available at Molecules 2018, 23, 3270; doi:10.3390/molecules23123270

(in aqueous solution, molecular concentration, different ratios of the two molecules) are reported very rarely [29–31]. However, the number of molecules in the unit volume, H_2O molecules and the interaction between different corrosion inhibitor molecules have important influences on the adsorption behavior. Therefore, the molecular dynamics simulation of the corrosion inhibitors mixture considering the H_2O molecule, corrosion inhibitor composition and concentration should be addressed.

In this paper, a derivative of pyridine, 4-methylpyridine (4-MP) and its quaternary ammonium salts (4-PQ), and sulfur-containing compounds including thiourea (TU) and mercaptoethanol (TZ) were selected to deduce synergistic effect in CO_2-saturated 3.5 wt.% NaCl solution by weight-loss method, open circuit potential (OCP), electrochemical impedance spectroscopy (EIS), potentiodynamic polarization and scanning electron microscopy (SEM). The synergistic mechanism was proposed based on the electrochemical results analysis, quantum chemical parameters calculation and molecular dynamics (MD) simulation.

2. Experimental

2.1 Materials

The molecular structures of 4-MP, 4-PQ, TU and TZ and the synthesis method are shown in Fig. 1. 4-PQ was synthesized by chemical reaction between 4-MP and benzyl chloride at 110°C for 4 hours.

Test specimen used in this study was Q235 steel with the following composition (wt.%):C 0.16, Si 0.30, Mn 0.53, P 0.015, S 0.004 and Fe balance. The corrosion medium was 3.5 wt.% NaCl solution, which prepared using analytical grade NaCl and deionized water.

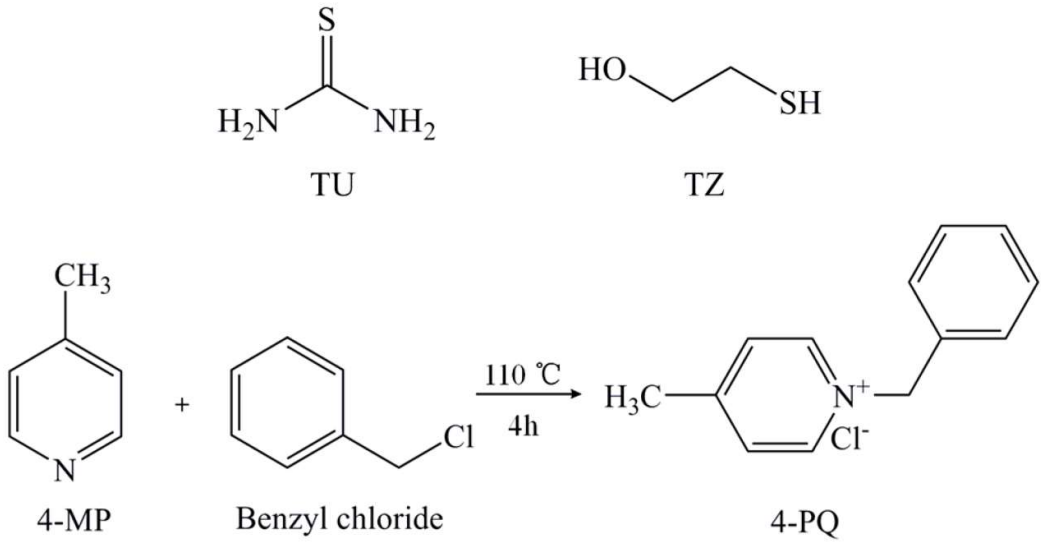

Fig. 1. Molecular structures of TU, TZ, 4-MP, 4-PQ and chemical reaction of quaternization.

2.2 Weight loss measurement

The carbon steel sheet of 40mm×13mm×2mm was abraded with a range of sandpaper (grade 280, 500, 1000) gradually, washed with deionized water, acetone, anhydrous ethanol, and then dried with a cold drier. After weighing by electronic analytical balance with sensitivity of ±0.1 mg. Then putted the sample into 100 ml corrosion solution containing with different inhibitors which deoxidized with N_2 for 0.5 hours and then saturated with carbon dioxide gas at atmospheric pressure by bubbling carbon dioxide for 0.5 hours at 60±1°C for 72 hours. After taking out the sample, immersed in the acid bath for a short time to remove the corrosion product, then cleaned, dried and re-weighed accurately.

The corrosion rate (*CR*) and inhibition efficiency (*IE*) were calculated from the following equation:

$$CR=\frac{\Delta W}{St} \qquad (1)$$

$$IE=\frac{CR_0-CR_{inh}}{CR_0}\times 100\% \qquad (2)$$

where ΔW is the average weight loss of three coupons, S is the sample area and t is the immersion time, CR_0 and CR_{inh} are the corrosion rate with and without inhibitors, respectively.

2.3 Electrochemical measurement experiments

All the electrochemical measurements were carried out on a *Corr Test* electrochemical workstation (Wuhan Corrtest Instruments Corp. LTD CS350), received and output experimental data by connecting computer software CorrTest (Ver 4.5). In this study, a conventional three electrodes test was carried out at 60°C, the working electrode (WE) is a cylindrical electrode wrapped in Teflon through the machine processing and the exposed test area was 0.5 cm^2. The saturated calomel electrode (SCE) was used as reference electrode (RE) through the connecting salt bridge, a platinum plate with a certain area was used as a counter electrode (CE). Before each experiment, the work electrode was polished by sandpaper (grade 500, 1000, 2000), dried with a cold drier after rinsing with deionized water and alcohol. The three electrode system was placed in the glass cell containing 100 mL test solution pumped N_2 for 0.5 hours to remove oxygen, then continuously bubbled steady flow of CO_2 throughout the experiment with and without corrosion inhibitors in the solution.

Firstly, the open circuit potential was measured to detect the change of the potential during immersing 2 hours. Electrochemical impedance spectroscopy measurements are performed after the open circuit potential over the frequency range from 0.01 Hz to 100 kHz at stable OCP with 10 mV AC amplitude. Then potentiodynamic polarization curves were conducted over a potential range from –400 mV to +400 mV (vs. OCP) at scan rate of 0.5 mV s^{-1}. The corrosion inhibition

efficiency (η_P and η_Z) was calculated from potentiodynamic polarization and EIS by means of the following equations, respectively:

$$\eta_P = \frac{I_{corr(0)} - I_{corr(inh)}}{I_{corr(0)}} \times 100\% \quad (3)$$

$$\eta_Z = \frac{R_{t(inh)} - R_{t(0)}}{R_{t(inh)}} \times 100\% \quad (4)$$

where $I_{corr(0)}$ and $R_{t(0)}$ represents corrosion current density and total resistance in the absence of inhibitors, $I_{corr(inh)}$ and $R_{t(inh)}$ stands for corrosion current density and total resistance of different inhibitor systems.

To study the order of adsorption in synergistic effect, polarization resistance tests were performed for different sequence of adding the one inhibitor at intervals of 40 minutes under a potential range from –10 mV to +10 mV (vs. OCP) at sweep rate of 0.2 mV s^{-1} at 10 minutes interval.

2.4 Surface analysis

The carbon steel sheets of 40mm×13mm×2mm were immersed in CO_2-saturated 3.5 wt.% NaCl solution without and with 2×10^{-4} mol/L mixed inhibitors of 4-PQ and TU (or TZ) which the molar ratio is 3:1 at 60°C for 72 hours, washed by deionized water, dried with a cold drier and then tested by SEM (EVO MA15, ZEISS).

2.5 Computational details

The M06-2x hybrid functional method were used to optimize the geometric structure of the inhibitor and calculate the quantum chemical parameters through the Gaussian 09 software package. The relevant quantum chemical parameters including energies of LUMO (E_{LUMO}) and HOMO (E_{HOMO}), energy gap (ΔE), absolute chemical hardness (η), electrochemical potential (μ), electronegativity (χ), the number of electron transfer (ΔN), electrophilicity index (ω) for four inhibitors were considered.

Molecular mechanics simulation was performed in the Forcite module by

Peer-reviewed version available at Molecules 2018, 23, 3270; doi:10.3390/molecules23123270

Materials Studio 8.1 software. The Geometry optimized function was used to optimize the geometry of five combinations containing 4-PQ and TU at different molar ratios in the water - Fe (1 1 0) surface system under the force field of COMPASS, making the entire system configuration more reasonable. Smart optimization algorithm was selected included the convergence standard was set to 2×10^{-5} kcal/mol and the maximum number of optimized steps was 20000 steps. The molecular dynamics (MD) simulation using the dynamics function to study the interaction between five combinations and Fe (1 1 0) surface in a simulation box (27.3 Å×27.3 Å×120.5 Å) with periodic boundary conditions to model a representative part of the interface devoid of any arbitrary boundary effects. Normal ensemble (NVT) was selected, and the Andersen thermostat was used to control the temperature at 333 K. The initial velocity of each particle was generated by the Maxwell-Boltzmann distribution and the Newton's equation of motion was calculated by the Velocity Verlet algorithm. The van der waals interaction and electrostatic effect were calculated by the Atom Based method and the Ewald method under 15 Å cut-off distance, respectively.

3. Results and discussion

3.1 Weight loss measurements

The corrosion inhibition effect of 4-MP, 4-PQ, TU, TZ and their mixture with different molar ratios at 2×10^{-4} mol/L for Q235 steel in CO_2-saturated 3.5 wt.% NaCl solution were studied by weight loss test at 60°C for 72 hours immersion, as shown in Table 1 and Fig. 2. Table 1 shows that 2×10^{-4} mol/L 4-MP or 2×10^{-4} mol/L 4-PQ has poor inhibition effect, while single TU or TZ can reduce the corrosion rate at the same concentration, and the inhibition efficiency reaches 77.5% and 77.6% respectively, there is no distinct difference between the inhibition efficiency of TU and TZ. From

Fig. 2, it indicates that the synergistic effects of 4-PQ with sulfur-containing compounds are better than that of 4-MP. The IE% of the compounded inhibitors are much higher than the sum of the IE% of individual 4-PQ and TZ or TU. The maximum values of IE% reach 89.3% and 93.1% when the molar ratio of 4-PQ and TZ or TU are all 3:1. For the synergistic system of 4-PQ and sulfur-containing compounds, the value of IE% is reduced with the molar ratio of sulfur-containing compounds increased.

Table 1. Corrosion rate and inhibition efficiency obtained from weight loss measurement of Q235 steel with different individual inhibitor in CO_2-saturated 3.5 wt.% NaCl solution at 60°C.

Inhibitors	CR ($g/m^2 \cdot h$)	IE (%)
blank	0.345	-
4-MP	0.341	1.4
4-PQ	0.335	2.7
TU	0.078	77.5
TZ	0.076	77.6

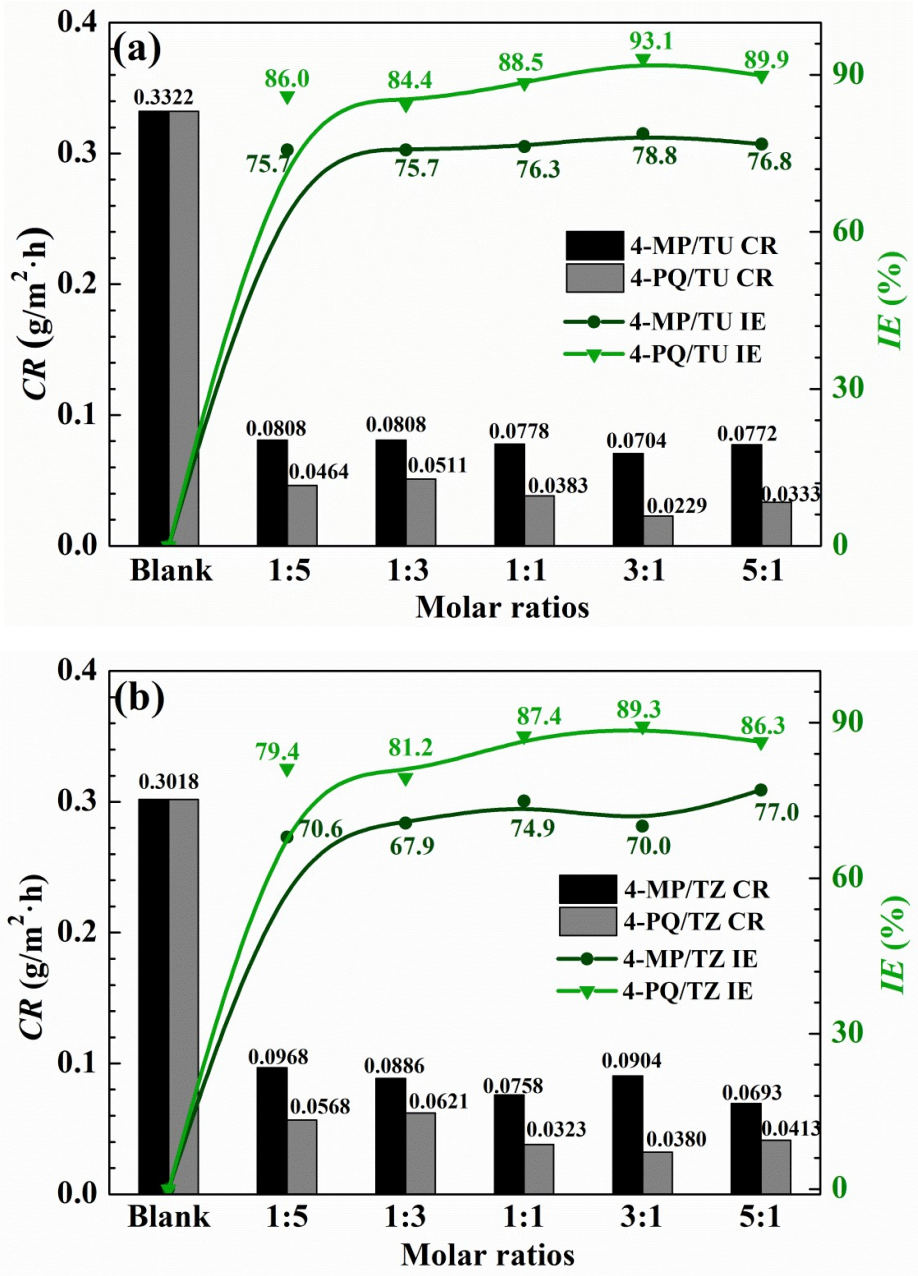

Fig. 2. Corrosion rate and inhibition efficiency obtained from weight loss measurement of Q235 steel with different mole ratios of (a) 4-MP (4-PQ)/TU and (b) 4-MP (4-PQ)/TZ in CO_2-saturated 3.5 wt.% NaCl solution at 60°C.

3.2 Open circuit potential monitoring

The open circuit potential measurement is performed at beginning to ensure potentiodynamic polarization and impedance measurements under the stable system,

the results are shown in Fig. 3. Fig. 3(a) shows the results of OCP without and with single 4-PQ, TZ and different molar ratios of 4-PQ and TZ immersed in CO_2-saturated 3.5 wt.% NaCl solutions for 2 hours. Fig. 3(b) shows the results for the composite inhibitors of 4-PQ and TU. In inhibitor-free solution, due to the dissolution of the metal, the potential is always more negative than the initial immersion time (t=0s). In the presence of different molar ratios of inhibitors, the OCP shifts more positive value, because inhibitors adsorb on the metal surface. After about 1500s, the potential reaches a steady value, and it is higher than lack of inhibitor, indicating that the metal corrosion is protected by inhibitors [32]. Comparing to single 4-PQ and single TU or TZ, the steady-state values of OCP with a large amount of TU or TZ are closed to single TU or TZ curve. This progressive positive of steady state potential with the proportion of 4-PQ increasing, is closed to single 4-PQ curve at the molar ratios of 4-PQ and TU or TZ are 1:1 and 5:1. However, under a certain ratio, the potential can reach the most positive value. These results indicate that the existence of a synergistic effect between 4-PQ and TU or TZ, and the molar ratio of 3:1 has the best effect of 4-PQ and TU or TZ.

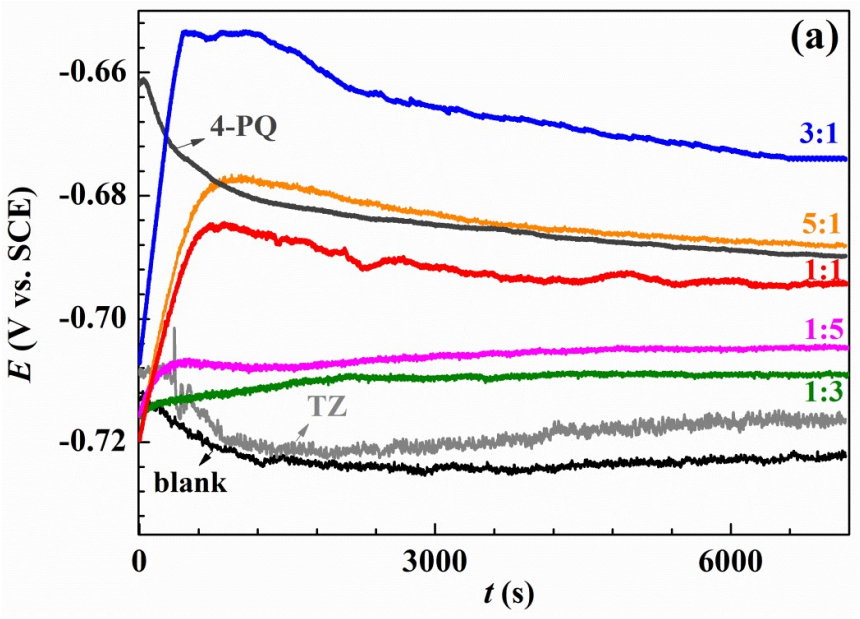

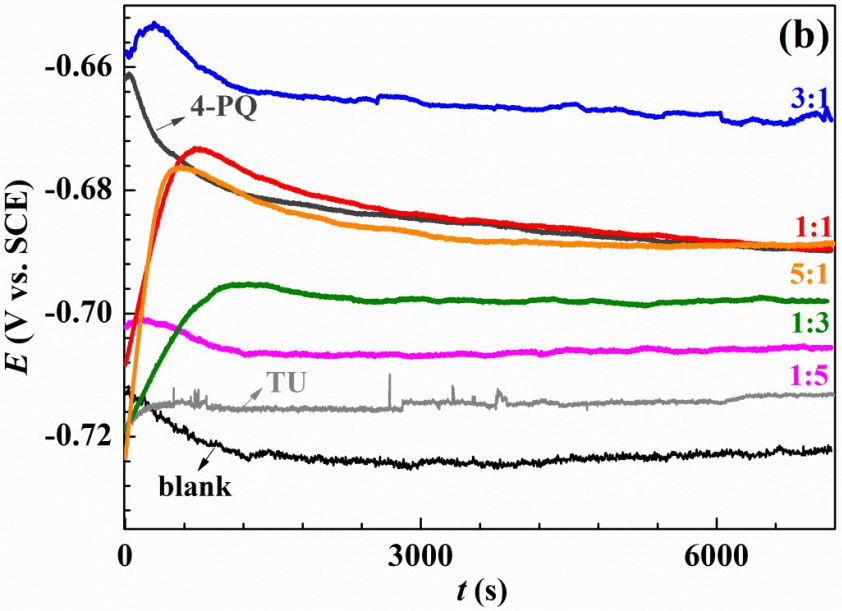

Fig. 3. Variation of the open circuit potential with immersion time recorded of Q235 steel in CO_2-saturated 3.5 wt.% NaCl solution at 60°C without and with (a) single inhibitor 4-PQ or TZ, and different molar ratios of 4-PQ and TZ; (b) single inhibitor 4-PQ or TU, and different molar ratios of 4-PQ and TU.

3.3 Potentiodynamic polarization

In order to further assess the synergistic effects between 4-PQ and sulfur-containing compounds, potentiodynamic polarization experiments were conducted for Q235 steel without and with 2×10^{-4} mol/L inhibitors at different mole ratios in CO_2-staturated 3.5 wt.% NaCl solutions at 60°C. Fig. 4 and Fig. 5 shows the potentiodynamic polarization curves of blank (without corrosion inhibitors) and different corrosion inhibitors, respectively. The fitting results of the polarization curves are shown in Table 2 and 3, respectively.

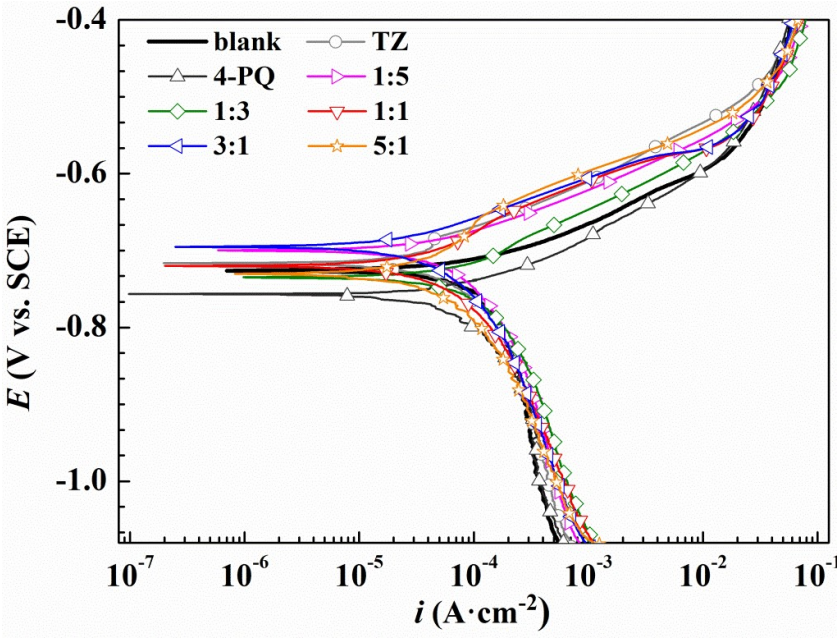

Fig. 4. Polarization curves of Q235 steel in CO_2-saturated 3.5 wt.% NaCl solution with or without different mole ratios of 4-PQ and TZ or individual inhibitor at 60°C.

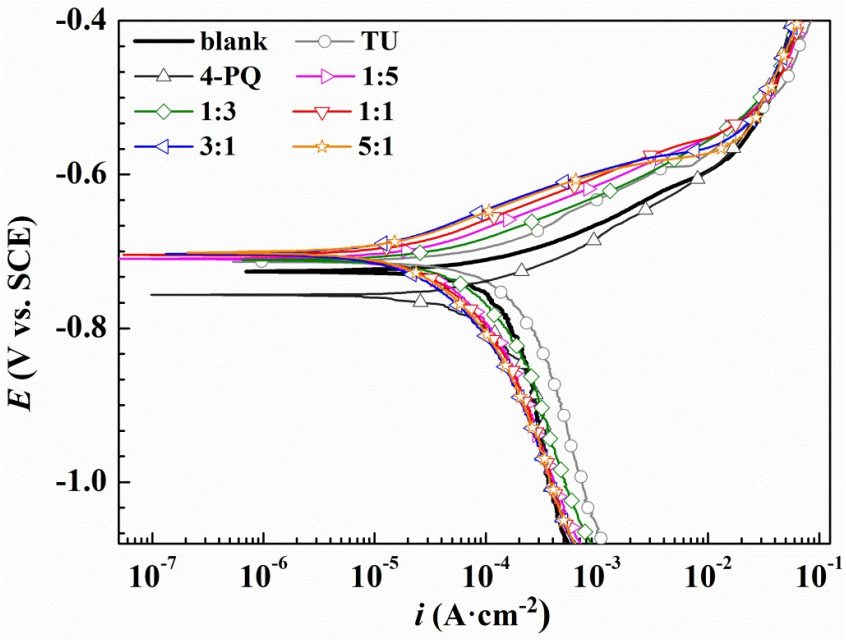

Fig. 5. Polarization curves of Q235 steel in CO_2-saturated 3.5 wt.% NaCl solution with or without different mole ratios of 4-PQ and TU or individual inhibitor at 60°C.

Peer-reviewed version available at *Molecules* **2018**, *23*, 3270; doi:10.3390/molecules23123270

Table 2. Polarization parameters of Q235 steel in CO_2-saturated 3.5 wt.% NaCl solution with or without different mole ratios of 4-PQ and TZ or individual inhibitor and at 60°C.

Inhibitors	b_a (mV)	$-b_c$ (mV)	E_{corr}(V)	I_{corr}(μA·cm^{-2})	η_P(%)
Blank	70	557	-0.726	136.7	
TZ	193	379	-0.717	59.3	56.6
4-PQ	80	412	-0.756	114.6	16.2
1：5	63	173	-0.713	56.5	58.6
1：3	82	181	-0.725	90.9	33.5
1：1	95	177	-0.710	50.3	63.2
3：1	60	107	-0.703	28.4	79.2
5：1	110	165	-0.711	48.2	64.7

Table 3. Polarization parameters of Q235 steel in CO_2-saturated 3.5 wt.% NaCl solution with or without different mole ratios of 4-PQ and TU or individual inhibitor at 60°C.

Inhibitors	b_a (mV)	$-b_c$ (mV)	E_{corr}(V)	I_{corr}(μA·cm^{-2})	η_P(%)
blank	70	557	-0.726	136.7	
TU	193	379	-0.714	69.2	49.4
4-PQ	80	412	-0.756	114.6	16.2
1：5	68	188	-0.710	43.4	68.2
1：3	67	206	-0.711	50.2	63.3
1：1	73	172	-0.705	28.3	79.2
3：1	79	159	-0.703	20.5	85.0
5：1	82	169	-0.701	24.1	82.3

As shown in Fig. 4, comparing to blank solution, the corrosion potential (E_{corr}) values of Q235 steel moves towards positive slightly, and anodic reaction are inhibited with added 4-PQ and TZ at molar ratio of 1:5, 1:3, 1:1, 3:1 and 5:1, implicating inhibitors adsorb on the metal surface to retard anodic dissolution of mild steel and suppress cathodic reduction simultaneously. Therefore, the composite inhibitors of 4-PQ and TZ are the mixed-type inhibitors which preferentially

suppressed the anodic process of corrosion. Table 1 indicates corrosion current density (I_{corr}) values of 1:1, 3:1 and 5:1 have a more remarkable decline than blank and individual inhibitor. Especially, the highest inhibition efficiency reaches 79.2% at the molar ratio is 3:1. However, when the molar ratio of 4-PQ and TZ is 1:3 or 1:5, the inhibition efficiency is better than adding 4-PQ alone, but lower than adding TZ alone. Therefore, 4-PQ needs to add a certain amount to promote synergistic effect in the composite inhibitors.

From Fig. 5 and Table 3, the polarization curve results of 4-PQ and TU are similar to the mixture of 4-PQ and TZ, but the synergistic inhibition efficiency is better than 4-PQ and TZ. Various of cathodic curves overlap with the blank, however, the shape of anodic curves changes greatly. The anode curve reflects the action of inhibitors. These can be divided into three regions, the slopes rapidly increases in the first region (< 100mv vs OCP), and this process shows that the inhibitors adsorbs on the metal surface and hinders the metal dissolution reaction of the anode. The second region (100~150mv vs OCP) has a slow growth potential and reflects the dynamic adsorption process of inhibitors on the metal surface. The third area (> 150mv vs OCP) coincides with the blank, indicating that the inhibitor completely separates from the metal surface. The highest inhibition efficiency is 86.5% in the present of 3:1 at 2×10^{-4} mol/L, and the inhibition efficiency of single 4-PQ and TU is only 16.2% and 49.4% respectively. Thus it can be seen adding sulfur-containing compounds have a good synergistic effect with 4-PQ for Q235 in CO_2-saturated 3.5 wt.% NaCl solution.

The synergistic corrosion inhibition effect of composite inhibitors with different molar ratios in the following order: 3:1 > 5:1 > 1:1 > 1:5 > 1:3 (4-PQ: TU or TZ). Although the values of IE% are different by different test methods, the results

obtained by polarization test show a good agreement with weight loss method.

3.4 Electrochemical impedance spectroscopy measurements

The effect of the mixture of 4-PQ and sulfur-containing compounds on the Nyquist and Bode plots for mild steel in CO_2-saturated 3.5 wt.% NaCl solution at 60°C are presented in Fig. 6. As seen from Nyquist plots, the working electrode immersed in different mole ratios all have a depressed semicircle with a center under the real axis at high frequency range, it is generally attributed to the roughness of the electrode surface, the uneven distribution of the carbon steel surface or the adsorption of the inhibitors on the surface of carbon steel [33,34]. In the whole frequency range, appearance of capacitive semicircles as observed in all Nyquist spectra is attributed to charge-transfer reaction and double layer capacitance. As labeled in Fig. 6(a), the diameter of 1:3 is less than 1:5 for the mixture of 4-PQ and TZ, but both of them are smaller than the diameter of TZ alone, which means the inhibition efficiency will be dominated by TZ and the synergistic effect with 4-PQ will be weak if TZ hold the main proportion. Then, the diameter increases significantly with the proportion of 4-PQ increased. As seen by Fig. 6(b), the curve of 4-PQ mixed with TU at different molar ratios is the same as mixed with TZ, but the semicircles diameter is larger than mixture of 4-PQ and TZ. Notably, the diameter of semicircle is the largest when the molar ratio of 4-PQ and TZ (or TU) is 3:1.

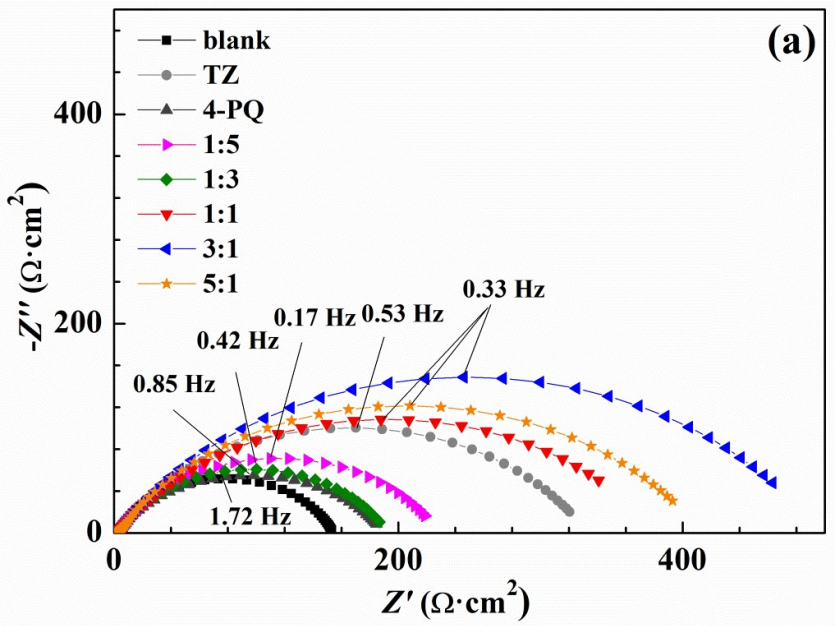

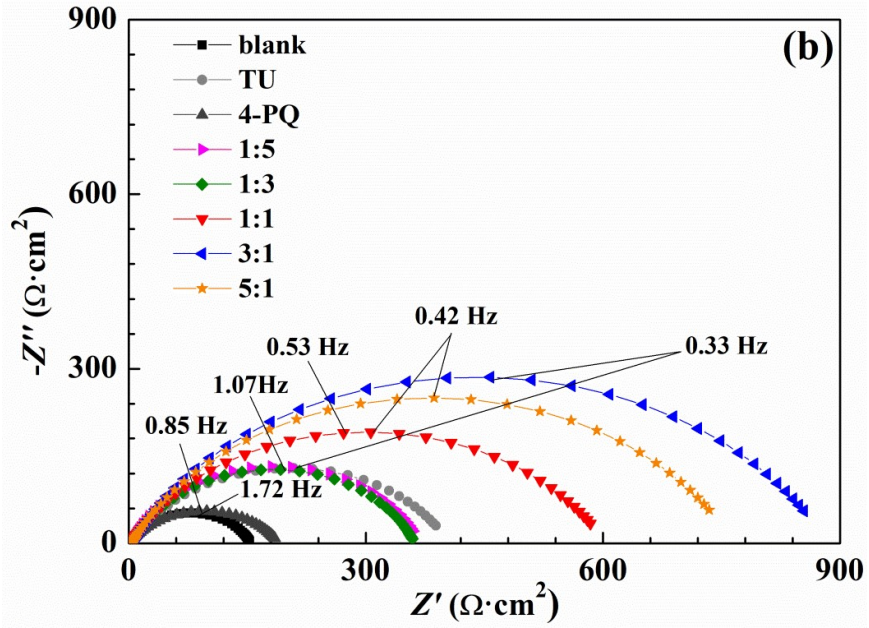

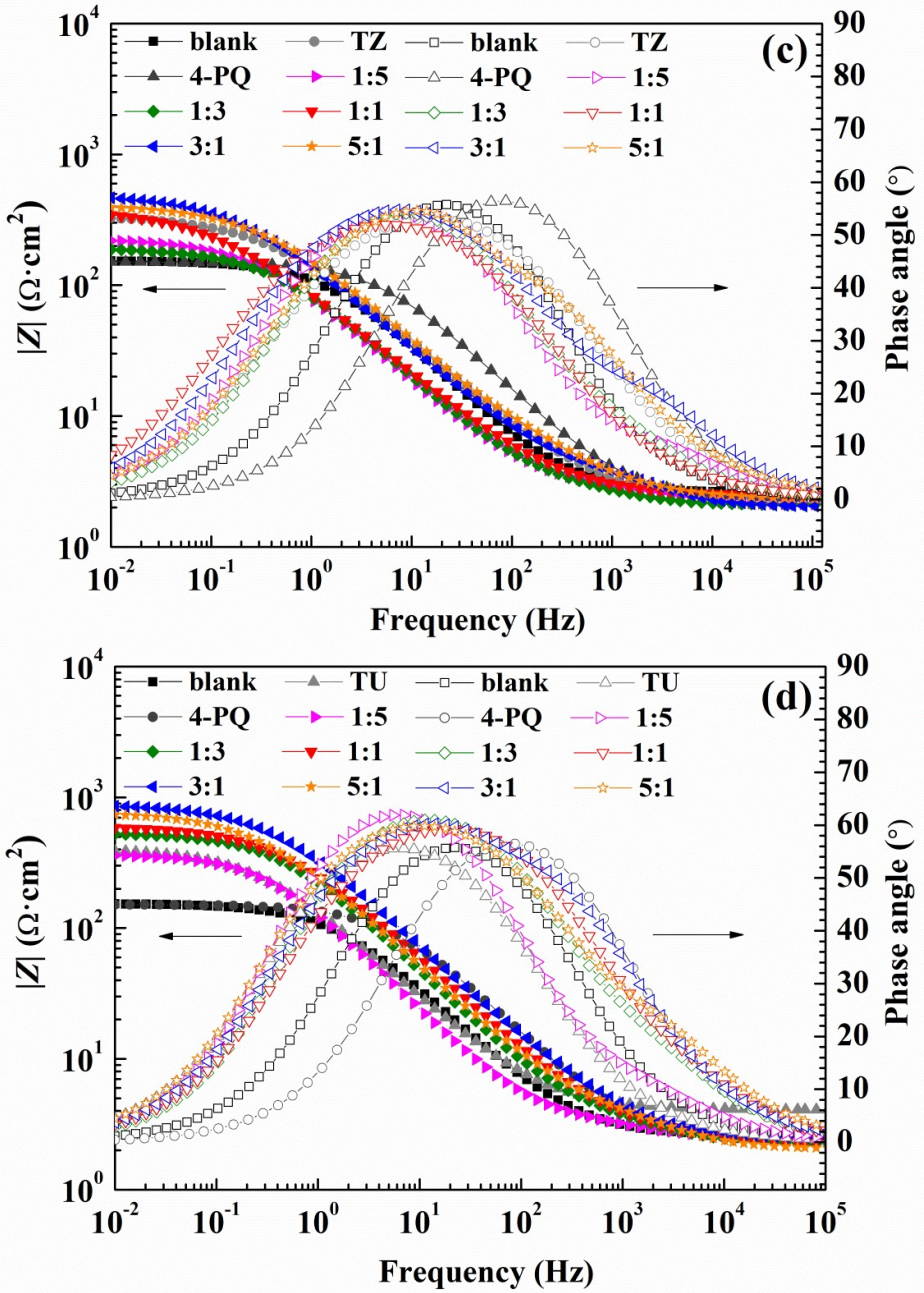

Fig. 6. Nyquist (a), (b) and (c), (d) Bode plots of Q235 steel in CO_2-saturated 3.5 wt.% NaCl solution with or without different mole ratios of 4-PQ and sulfur-containing compounds or individual inhibitor at 60°C.

The absolute value of the impedance increases with the addition of inhibitors compared with the blank solution in Bode plot (Fig. 6c and d) at low frequency.

Simultaneously, phase angle plot were observed to follow similar trend as Nyquist and Bode plots. Fig. 7 shows an equivalent circuit diagram of blank solution (Fig. 7a) and an equivalent circuit diagram of two time constants used to fit data well for solution containing mixed corrosion inhibitors (Fig. 7b). Here, R_s stands for the solution resistance, R_{ct} is the charge transfer resistance, R_f represents the resistance of the protective inhibitor film formed on Q235 surface, CPE_{dl} and CPE_f represent constant phase element of double layer and constant phase element of adsorption film, respectively [11,35,36]. The extracted parameters from EIS are summarized in Table 4 and Table 5. The values of C_{dl} and C_f are calculated from Y_0 and n as follows [37,38]:

$$C = Y_0(2\pi f_{max})^{n-1}$$

where Y_0 represents the magnitude of the CPE, f_{max} is the frequency at the maximum value of the imaginary component of the impedance spectrum, and n is the deviation parameter in regard to the phase shift.

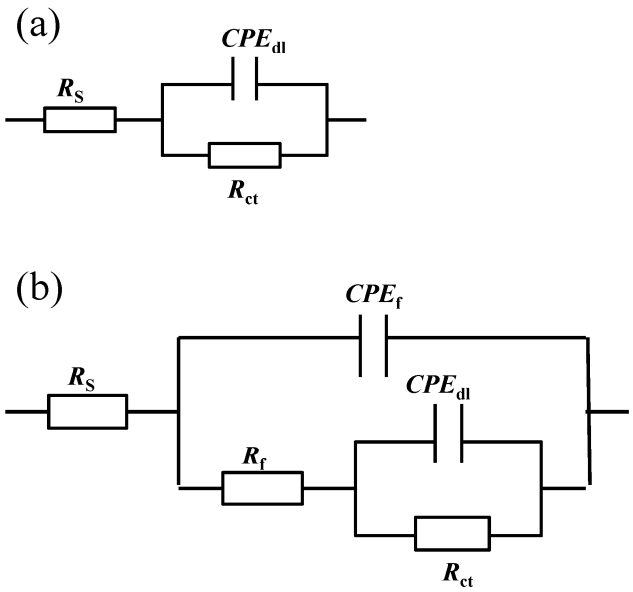

Fig. 7. The equivalent circuit used to model the electrochemical behavior of Q235 steel in CO_2-saturated 3.5 wt.% NaCl solution containing (a) blank and (b) individual

and mixture of 4-PQ and sulfur-containing compounds.

The values of R_f and R_{ct} are increased with the addition of composite inhibitors compared to the blank solution. Further, the value of R_t (R_f +R_{ct}) reached the maximum when the content of 4-PQ makes the proportion reached 3:1 with sulfur-containing compounds. On the other hand, the minimum value of C_{dl} indicates that the thickness of the double layer is increased to the maximum or the dielectric constant is reduced to the minimum due to the adsorption of the inhibitor [38]. The mixture of 4-PQ and TU has better performance and inhibition efficiency reaches 82.8% at 3:1, it implies the corrosion inhibitors formed complete and dense film by the two substances. All of above results reveal the synergistic effect of 4-PQ with sulfur-containing compounds depends on molar proportion of composite inhibitors.

Table 4. Equivalent circuit parameters and inhibition efficiency (IE) obtained from EIS measurements of Q235 steel in CO_2-saturated 3.5 wt.% NaCl solution with or without different mole ratios of 4-PQ and TZ or individual inhibitor at 60°C.

Inhibitors	R_s ($\Omega\cdot cm^2$)	R_f ($\Omega\cdot cm^2$)	R_{ct} ($\Omega\cdot cm^2$)	C_f ($\mu F/cm^2$)	n_f	C_{dl} ($\mu F/ cm^2$)	n_{dl}	R_t ($\Omega\cdot cm^2$)	η_Z (%)
Blank	2.58	-	151.7		-	115.9	0.80	151.7	-
TZ	2.26	0.68	335.7	99.8	0.68	73.7	1	336.4	54.95
4-PQ	2.23	0.97	197.7	90.9	0.98	85.5	0.78	198.7	23.65
1:5	2.12	1.95	225.1	16.0	0.89	74.1	0.71	226.1	32.89
1:3	2.09	0.34	189.7	111.7	0.84	94.3	0.70	190.5	20.35
1:1	2.43	1.02	377.9	40.3	0.66	67.3	0.75	378.9	59.97
3:1	2.03	2.50	491.1	13.9	0.84	64.4	0.68	493.6	69.27

5:1	2.28	1.76	410.0	24.7	0.66	73.5	0.93	411.8	63.17

Table 5. Equivalent circuit parameters and inhibition efficiency (IE) obtained from EIS measurements of Q235 steel in CO_2-saturated 3.5 wt.% NaCl solution with or without different mole ratios of 4-PQ and TU or individual inhibitor at 60°C.

Inhibitors	R_s ($\Omega \cdot cm^2$)	R_f ($\Omega \cdot cm^2$)	R_{ct} ($\Omega \cdot cm^2$)	C_f ($\mu F/ cm^2$)	n_f	C_{dl} ($\mu F/ cm^2$)	n_{dl}	R_t ($\Omega \cdot cm^2$)	η_Z (%)
Blank	2.58	-	151.7	-	-	115.9	0.80	151.70	-
TU	2.03	1.54	323.2	21.1	0.71	57.0	0.86	324.74	53.06
4-PQ	2.23	0.97	198.7	90.9	0.98	85.5	0.78	199.67	23.65
1:5	2.47	1.47	363.5	46.3	0.81	89.9	0.79	364.97	58.47
1:3	2.23	2.56	349.9	54.9	0.79	37.6	0.78	352.46	56.96
1:1	2.28	1.77	599.6	5.7	0.92	56.4	0.70	601.37	74.76
3:1	2.44	2.66	879.6	1.3	0.60	42.5	0.72	882.26	82.80
5:1	2.04	1.66	759.50	18.8	0.79	51.2	0.72	761.16	80.12

3.5 Synergistic mechanism

In order to further study the synergistic mechanism of mixed corrosion inhibitors, the linear polarization resistance method was used. Fig. 8 shows the OCP and polarization resistance analysis (calculated from polarization curves vs. time) with and without 4-PQ and TU in different addition sequence. As can be seen from Fig. 8(a), curve 1 and 4 are blank solution and adding mixed corrosion inhibitors at t=0 s for comparing, respectively. Curve 2 is adding single TU at t=0 s, the values of OCP are closed to curve 1 and increase slowly, then adding another corrosion inhibitor 4-PQ at t=2400 s, the OCP curve sharp rises. Curve 3 is adding in reverse order, it is

near to curve 4 at the beginning. However, all curves expect blank solution (curve 1) are stabilized at the close-set positions and all the solutions contained 2×10^{-4} mol/L mixed inhibitors of 4-PQ and TU with 3:1 in the end.

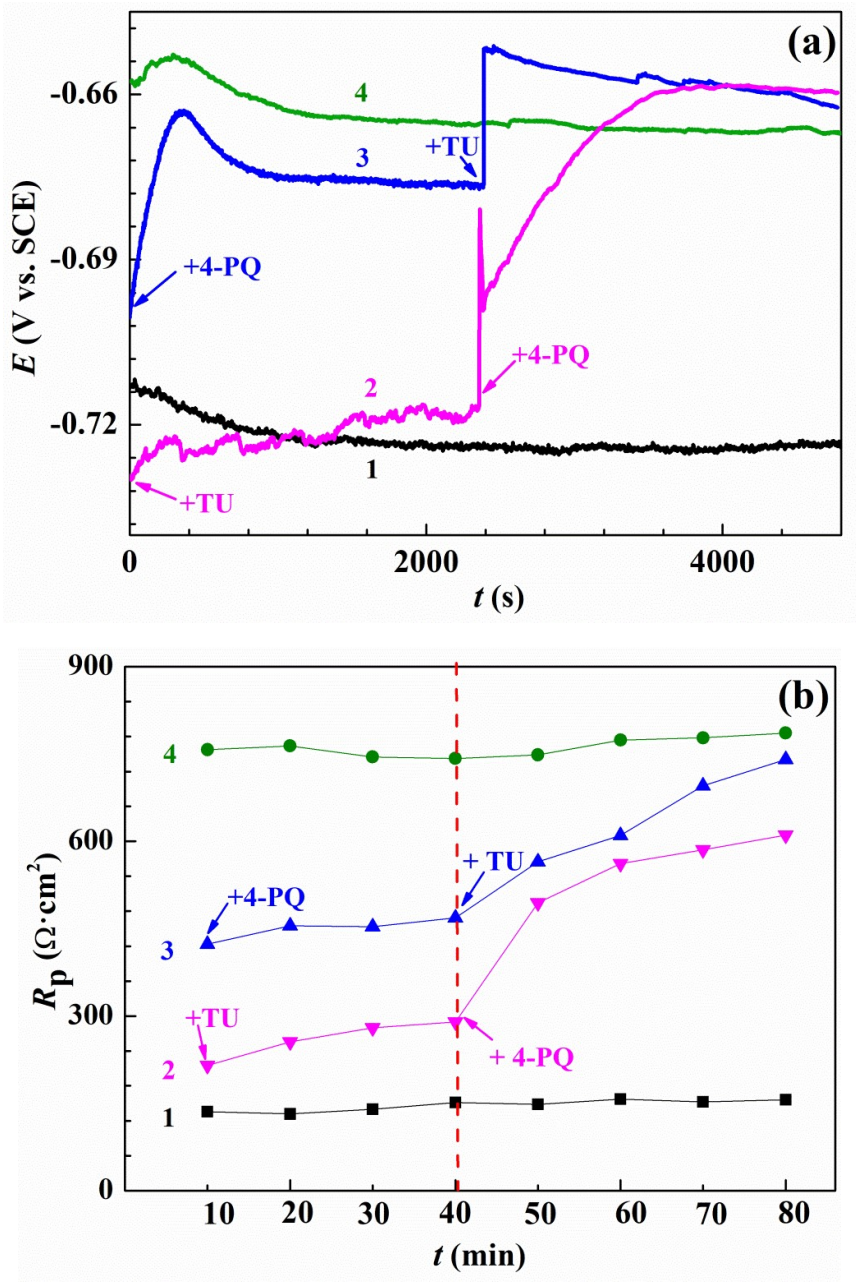

Fig. 8. OCP measurements and polarization resistance analysis: (a) variation of the open circuit potential and (b) values of polarization resistance without or with 4-PQ and TU in different addition of sequence. Curve 1 and 4 in all the graphs stands for

Peer-reviewed version available at Molecules 2018, 23, 3270; doi:10.3390/molecules23123270

blank and adding corrosion inhibitors mixture contained 4-PQ and TU at the beginning, respectively. Curve 2 represents adding TU at beginning, then adding 4-PQ at the time of 40th minutes. Curve 3 represents adding 4-PQ at beginning, then adding TU at the time of 40th minutes.

The resistance curves of direct current polarization measured for 4-PQ and TU of 3:1 with different addition sequence are shown in Fig. 8(b). As seen in Fig. 8(b), the value of polarization resistance (R_p) of the corrosion inhibitors mixture added at t=0 min remained constant (785 $\Omega \cdot cm^2$) during the test, and is closed to R_t from the impedance test results [39]. In the first 40 minutes of adding single corrosion inhibitor, the R_p is lower than the mixed corrosion inhibitors. The R_p of adding single 4-PQ that makes up three quarters of 2×10^{-4} mol/L is 458 $\Omega \cdot cm^2$, and then TU is added at the 40th minute, which the curve of R_p shifted steep immediately. Ultimately, the steady value is consistent with the curve of addition together at the beginning. On the other hand, the R_p of a quarter of 2×10^{-4} mol/L single TU is stable at 280 $\Omega \cdot cm^2$, and then added another inhibitor 4-PQ, the R_p increases a bit and is lower than the previous situation. It reveals the concentration of TU is too low to form the dense inhibitor film on the metal surface after preferential addition, and further formed the crystalline compound with adding 4-PQ which accumulated above the film of TU [40], and 4-PQ cannot fill the active site to form a dense inhibitor film, resulting in the resistance is much lower than mixtures. All of above results indicate adsorption order has an effect on the synergistic effect of composite inhibitors.

3.6 Scanning electron microscopy characterization

Fig. 9 presents photographs of the corrosion morphologies of Q235 steel immersion in CO_2-saturated 3.5 wt.% NaCl solution for 72 hours at 60°C in the

absence and presence of the optimum mole ratio of mixed inhibitors. The Fig. 9(a) and (b) are blank solutions and added single 4-PQ in solution, respectively, (c) and (d) are the mixture of 4-PQ and sulfur-containing compounds with molar ratio of 3:1. It can be seen that homogeneous corroded area are observed on the sample surface in the blank solution (without corrosion inhibitors), as the same as added single 4-PQ. The surface of the sample immersed in solution with mixed inhibitors is smooth and uniform, the corrosion degree is slowed down significantly. It illustrates that mixed inhibitors of 4-PQ and sulfur-containing compounds with the molar ratio of 3:1 formed a compact protective film on the surface of Q235 steel, inhibiting the corrosion of carbon steel in this medium.

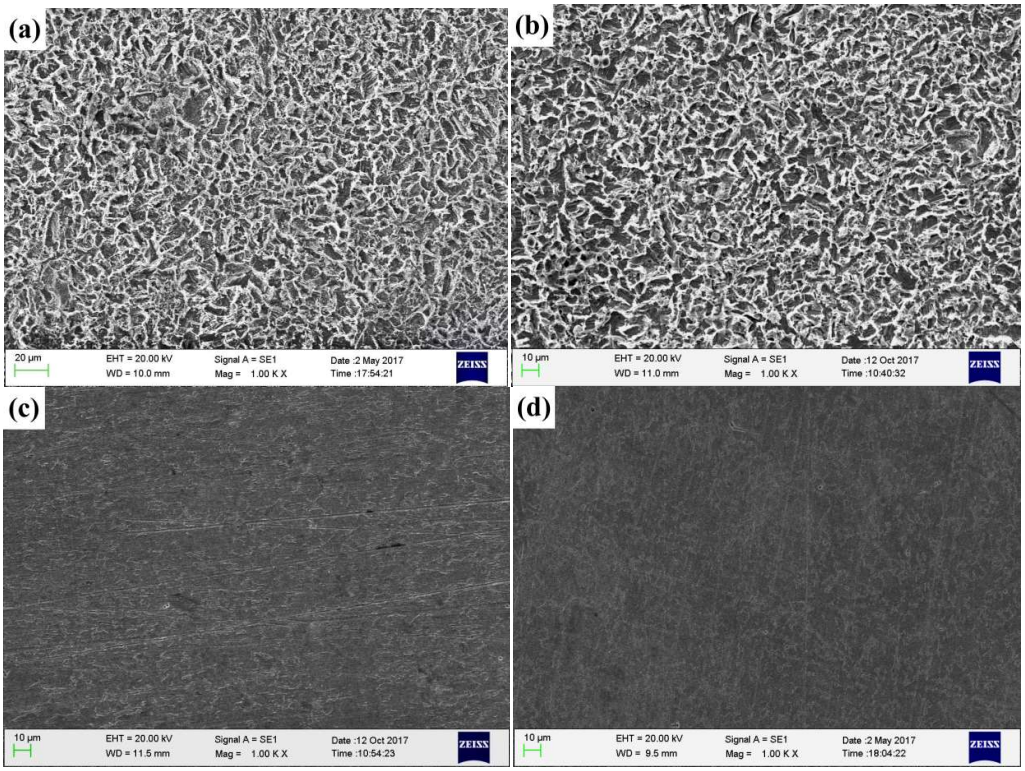

Fig. 9. The corrosion morphology of Q235 steel obtained after immersion in CO_2-saturated solution for 72h: (a) without inhibitors, (b) with 2×10^{-4} mol/L 4-PQ, (c) with 2×10^{-4} mol/L 4-PQ and TZ at 3:1, (d) with 2×10^{-4} mol/L 4-PQ and TU at 3:1.

3.7 Quantum chemical calculation

Quantum chemical calculation is a useful method to explain the theory of the adsorption of corrosion inhibitor molecules on the metal surface and the interaction between molecules. The parameters from quantum chemical calculation can be used to describe the global reaction activity of inhibitor molecules, included the highest occupied molecular orbital (HOMO), lowest unoccupied molecular orbital (LUMO). It is easier to give electrons with the value of E_{HOMO} increasing. For another, the lower of E_{LUMO} indicates the energy decreases to accept the electron easily [41].

The frontier molecule orbital density distributions of the pyridine derivatives compounds (4-MP) and its quaternary ammonium salt (4-PQ) and two kinds of sulfur-containing compounds (TU and TZ) are shown in Fig. 10. It can be seen that the distribution of the frontline orbit is mainly concentrated in the heterocyclic ring containing nitrogen and the sulfur atom. The quantum chemical calculation parameters of these inhibitors are shown in Table 6, the most imperative parameter is energy difference (ΔE) between E_{HOMO} and E_{LUMO}, and the decrease in ΔE lead to the increase in the activity of reactive [42]. For four inhibitors, the ΔE of TU is the smallest and the next is 4-PQ, indicating the combination of 4-PQ and TU is better. It coincides with the actual experimental results.

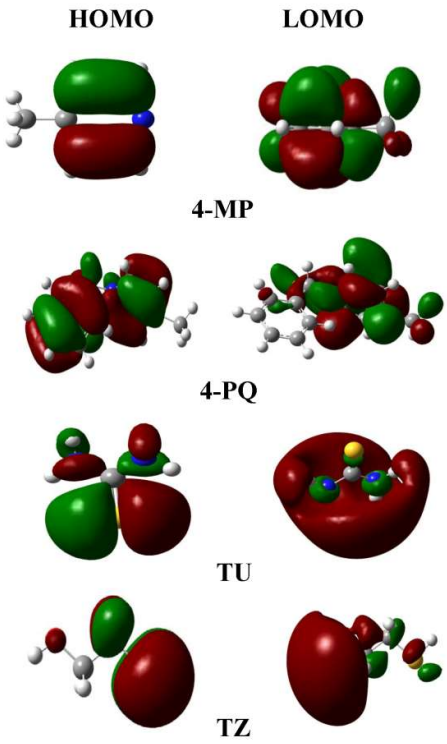

Fig. 10. Schematic representation of HOMO and LUMO molecular orbital of pyridine derivatives and sulfur-containing compounds (Color code: N, blue; S, yellow; C, gray; H, white).

Table 6. Calculated quantum chemical indices of pyridine derivatives and sulfur-containing compounds.

Inhibitor	E_{HOMO}	E_{LUMO}	ΔE	η	w	ΔN	χ	μ
4-MP	-8.648	0.069	8.717	4.358	2.111	0.311	4.289	-4.289
4-PQ	-8.123	-0.0014	8.121	4.061	2.032	0.362	4.062	-4.062
TU	-7.255	-0.110	7.146	3.573	1.898	0.464	3.682	-3.682
TZ	-8.079	0.279	8.358	4.179	1.820	0.371	3.900	-3.900

3.8 Molecular dynamics simulation

Molecular dynamics simulations of the adsorption process of corrosion inhibitors mixture on Fe (1 1 0) surface under different condition are presented in Fig. 11. The MD simulation further proves the adsorption ability and configurations of these inhibitors at different molar ratios on metal surfaces. The side views of 4-PQ and TU reveals that the total number is 12 with the ratio of 1:5, 1:3, 1:1, 3:1, and 5:1 respectively. Some corrosion inhibitors are free in aqueous solution while the others are adsorbed on the Fe (1 1 0) surface at different molar ratios. The nitrogen-containing heterocyclic of 4-PQ provides the lone pairs of electrons to form covalent bonds with empty orbitals of iron, and flat adsorbs the active sites of the metal surface. The N and S atoms in the TU structure also play the same role.

It can be seen from the coverage degree of iron-based surface that the corrosion inhibitors mixture with molar ratio of 3:1 can achieve the maximum coverage and 1:3 is the minimum coverage. In addition, the adsorption stability of corrosion inhibitor molecules is studied by the adsorption energy of the corrosion inhibitor molecules. The higher absolute value of the adsorption energy implies the adsorption of the inhibitors is more stable on the metal surface, the inhibition effect is better and these inhibitor molecules have the stronger synergy. Adsorption energy ($E_{adsoption}$) is calculated as follows [43,44]:

$$E_{adsoption}=E_{total}-(E_{surface+solution}+E_{inhibitors+solution})-E_{solution}$$

where E_{total} is the total energy of the simulation system includes the iron crystal together with the adsorbed inhibitor molecules on the iron surface and the solution; $E_{surface+solution}$ stands for the total energy of the system without the inhibitors; $E_{inhibitors+solution}$ is the total energy of the system without the iron crystal; and $E_{solution}$ is designated as the total energy of the solution.

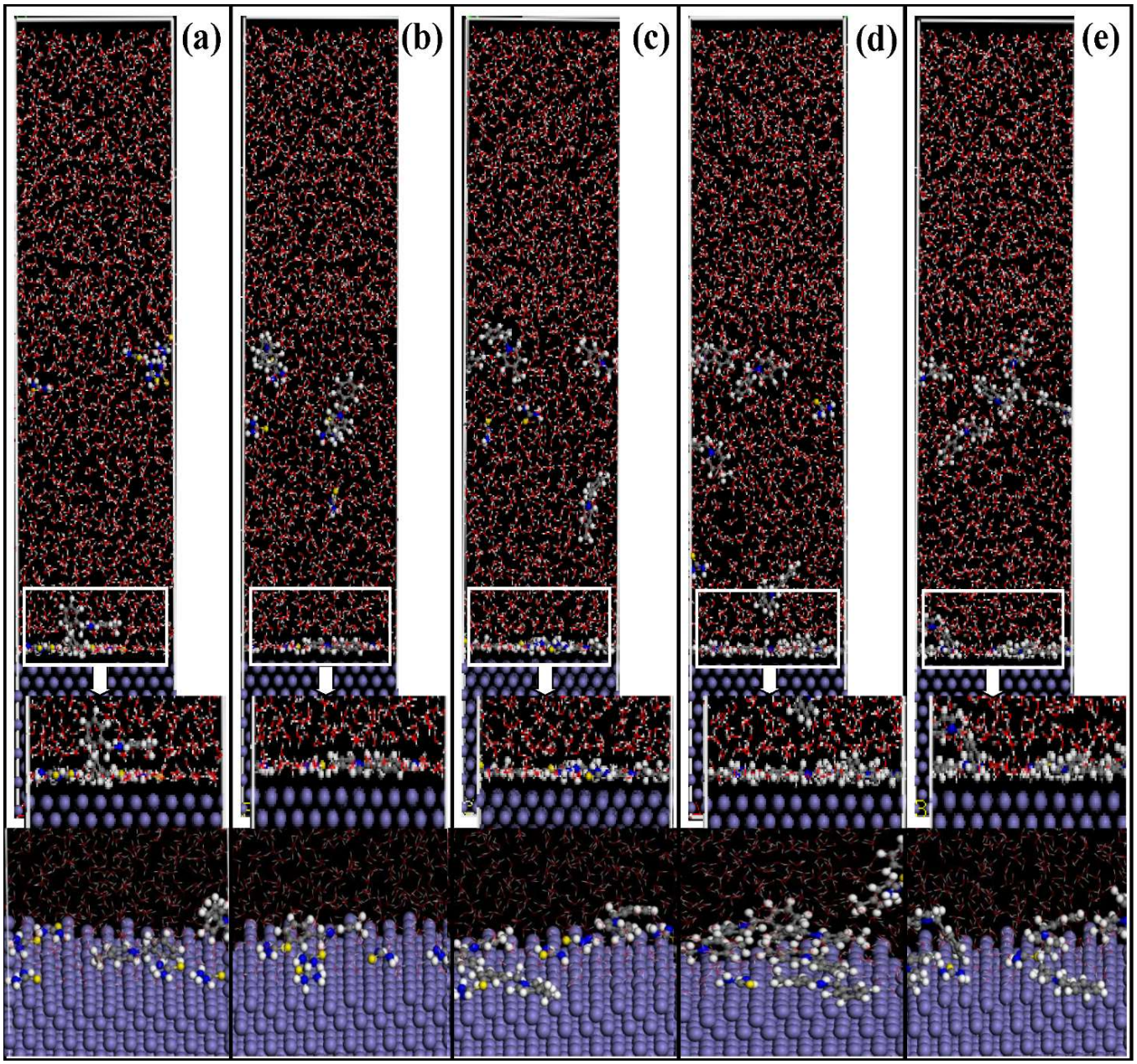

Fig. 11. Side views of the lowest energy adsorption configurations of 4-PQ and TU with different molar ratios (a) 1:5, (b) 1:3, (c) 1:1, (d) 3:1 and (e) 5:1 on Fe (1 1 0) calculated by MD simulations.

Table 7. The output obtained from MD simulations for the adsorption of 4-PQ and TU with different molar ratios.

4-PQ:TU	E_{total}	$E_{surface+solution}$	$E_{inhibitors+solution}$	$E_{solution}$	$E_{adsoption}$
1:5	-41105.7	-39365.3	-8953.9	-7518.03	-304.495
1:3	-40974.3	-39389	-8823.87	-7536.58	-297.995
1:1	-40556.2	-39237.3	-8347.31	-7508.61	-480.2
3:1	-39985.6	-38771.2	-7734.12	-7083.08	-563.43
5:1	-39856.7	-38861.6	-7606.54	-7157.9	-546.394

The results of 4-PQ and TU with different molar ratios by calculating are presented in the Table 7. The order of absolute value of $E_{adsoption}$ is 3:1>5:1>1:1>1:5>1:3, which indicates that the compounding molar ratio has a great influence on the synergistic effect of corrosion inhibitors mixture. There is a optimal ratio between the TU and 4-PQ molecules, the parallel adsorption ability become stronger and the inhibitors film is denser on Fe (1 1 0) surface with the number of 4-PQ increasing, bring about the best synergistic effect. However, it seen from the side view of 5:1, the adsorption points of TU are seized by 4-PQ, of which the number continued to rise. The number of adsorbed molecules decrease on the iron surface and voids appear easily to cause the low adsorption energy, that is why the corrosion inhibition effect deteriorates. The synergistic mechanism of the compound inhibitors is that the 4-PQ with a larger molecular structure and the small molecule TU occupy adsorption sites completely to form a dense adsorption film at the optimal ratio. This result is mutually verified with the experimental results. It is also noticed that these adsorbed molecules are not regularly arranged at the metal/water interface, which is quite different from the classic adsorption model.

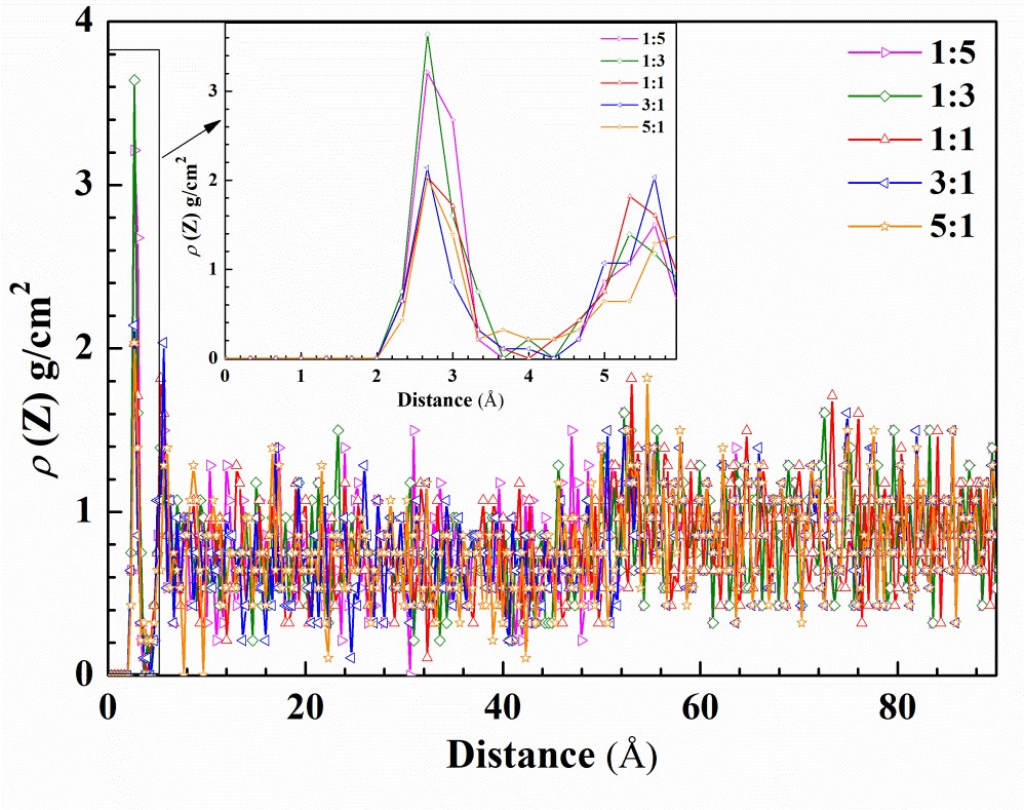

Fig. 12. Concentration profile for water molecules on the metal surface as a function of height with corrosion inhibitors at different molar ratios.

In order to quantitatively describe the protective effect of inhibitors film at different molar ratios, the concentration profile of water molecules was calculated in the absence and presence of corrosion inhibitors. As can be seen from the Fig. 12, the first concentration profile peak value of water molecules curve appears at a height of 2.6 Å from the iron surface. Obviously, under the molar ratio of 1:3, the water density distribution is the largest, followed by 1:5 and 1:1. This is due to a large number of TU molecules occupy active sites but small molecule structure can not fill the metal surface entirely and water molecules enter spacing at these molar ratios. At a molar ratio of 3:1, the peak of water molecule concentration profile is the smallest value and has narrower peak shape than other ratios with rising from the iron surface distance. It

shows that 4-PQ and TU have a high coverage at a molar ratio of 3:1 on the iron surface, which hinders the adsorption of water molecules and play a good protective effect. Rather, the number of large molecular that are adsorbed on the metal surface increasing lead to appear the voids under the molar ratio of 5:1, so that the small molecule cannot be filled and the water molecules concentration increases. The concentration profile of water molecules in the region of 3.8~4.8 Å from Fe (1 1 0) surface appears a trough with addition of inhibitors at different molar ratios, especially the concentration value of water molecules is close to zero at the molar ratio of 3:1. It indicates that the mixed inhibitors adsorbs on the Fe (1 1 0) surface and remove water molecules away from the metal surface. With the increase of the height from surface, the difference of reducing for the concentration profile of the water molecules indicates the mixed inhibitors acts as a role to impede the water molecules adsorbed on the metal surface within a range of distance.

4. Conclusions

(1) In the CO_2-saturated 3.5 wt.% NaCl solution, the inhibition effect of single 4-MP or 4-PQ is poor, but the corrosion inhibition effect is improved remarkably by using the mixed corrosion inhibitors with different molar ratios at 2×10^{-4} mol/L. It indicates there is a significant synergistic inhibition effect between 4-PQ and sulfur-containing compounds (TZ or TU) in such corrosive condition. Furthermore, the mixed corrosion inhibitors mainly influence on the anode process of carbon steel corrosion.

(2) The corrosion inhibition performance of the mixed corrosion inhibitors depends on the molar ratio between two mixed compounds and it respects to the following order: 3:1 > 5:1 > 1:1 > 1:5 > 1:3 (4-PQ: TZ or TU). At the molar ratio of 1:3 or 1:5, the corrosion inhibition behavior of the mixed corrosion inhibitors is similar

to the single TZ or TU, because the big amount of sulfur-containing compounds decreased the chance of 4-PQ molecule accesses to the metal surface. The synergistic corrosion inhibition effect between 4-PQ and sulfur-containing compounds increases with the increase of the content of 4-PQ in the mixed corrosion inhibitors, but the corrosion inhibition effect decreases after the molar ratio reaches 3:1.

(3) The mechanism of synergistic effects of the mixed corrosion inhibitors is revealed by electrochemical measurements, theoretical calculation and MD simulation. The large-volume pyridine derivatives compound molecules have a priority to adsorb on the metal surface, while the small sulfur-containing compounds molecules fill in vacancies. The two molecules are in plane adsorption on the metal surface, and a dense protective film can be formed when two compounds is at the proper molar ratio, performing good corrosion resistance.

Acknowledgements

We are grateful to the support of Sichuan Key Lab of Oilfield Materials [Grant No. X151517KCL32], Project Funding to Scientific Research Innovation Team of Universities Affiliated to Sichuan Province [Grant No. 18TD0012], Applied Basic Research Programs of Science and Technology Department of Sichuan Province [Grant No. 2017JY0044] and National Science and Technology Major Project [Grant No. 2017ZX05030-001].

References

[1] S. Nešić, Key issues related to modelling of internal corrosion of oil and gas pipelines - A review, Corros. Sci. 49 (2007) 4308–4338. doi:10.1016/j.corsci.2007.06.006.

[2] S. Nesic, J. Postlethwaite, S. Olsen, An electrochemical model for prediction of corrosion of mild steel in aqueous carbon dioxide solutions, Corros. 52 (1996) 280–294. doi:10.5006/1.3293640.

[3] J.K. Heuer, J.F. Stubbins, An XPS characterization of $FeCO_3$ films from CO_2 corrosion, Corros. Sci. 41 (1999) 1231–1243. doi:10.1016/S0010-938X(98)00180-2.

[4] M.B. Kermani, A. Morshed, Carbon dioxide corrosion in oil and gas production—a compendium, Corrosion. 59 (2003) 659–683. doi:10.5006/1.3277596.

[5] B.D.B. Tiu, R.C. Advincula, Polymeric corrosion inhibitors for the oil and gas industry : Design principles and mechanism, REACT. 95 (2015) 25–45. doi:10.1016/j.reactfunctpolym.2015.08.006.

[6] A.A. Olajire, Corrosion inhibition of offshore oil and gas production facilities using organic compound inhibitors - A review, J. Mol. Liq. 248 (2017) 775–808. doi:10.1016/j.molliq.2017.10.097.

[7] D.A. López, W.H. Schreiner, S.R. De Sánchez, S.N. Simison, The influence of inhibitors molecular structure and steel microstructure on corrosion layers in CO_2 corrosion: An XPS and SEM characterization, Appl. Surf. Sci. 236 (2004) 77–97. doi:10.1016/j.apsusc.2004.03.247.

[8] F.G. Liu, M. Du, J. Zhang, M. Qiu, Electrochemical behavior of Q235 steel in saltwater saturated with carbon dioxide based on new imidazoline derivative inhibitor, Corros. Sci. 51 (2009) 102–109. doi:10.1016/j.corsci.2008.09.036.

[9] P.C. Okafor, X. Liu, Y.G. Zheng, Corrosion inhibition of mild steel by ethylamino imidazoline derivative in CO_2-saturated solution, Corros. Sci. 51 (2009) 761–768. doi:10.1016/j.corsci.2009.01.017.

[10] P.C. Okafor, Y. Zheng, Synergistic inhibition behaviour of methylbenzyl quaternary imidazoline derivative and iodide ions on mild steel in H_2SO_4 solutions, Corros. Sci. 51 (2009) 850–859. doi:10.1016/j.corsci.2009.01.027.

[11] C. Georges, E. Rocca, P. Steinmetz, Synergistic effect of tolutriazol and sodium carboxylates on zinc corrosion in atmospheric conditions, Electrochim. Acta. 53 (2008) 4839–4845. doi:10.1016/j.electacta.2008.01.073.

[12] S.A. Umoren, M.M. Solomon, Synergistic corrosion inhibition effect of metal cations and mixtures of organic compounds: A Review, J. Environ. Chem. Eng. 5 (2016) 246–273. doi:10.1016/j.jece.2016.12.001.

[13] M. Heydari, M. Javidi, Corrosion inhibition and adsorption behaviour of an amido-imidazoline derivative on API 5L X52 steel in CO_2-saturated solution and synergistic effect of iodide ions, Corros. Sci. 61 (2012) 148–155. doi:10.1016/j.corsci.2012.04.034.

[14] M. Mobin, S. Zehra, M. Parveen, L-Cysteine as corrosion inhibitor for mild steel in 1 M HCl and synergistic effect of anionic, cationic and non-ionic surfactants, J. Mol. Liq. 216 (2016) 598–607. doi:10.1016/j.molliq.2016.01.087.

[15] R. Fuchs-Godec, Effects of surfactants and their mixtures on inhibition of the corrosion process of ferritic stainless steel, Electrochim. Acta. 54 (2009) 2171–2179. doi:10.1016/j.electacta.2008.10.014.

[16] J. Zhao, G. Chen, The synergistic inhibition effect of oleic-based imidazoline and sodium benzoate on mild steel corrosion in a CO_2 -saturated brine solution, Electrochim. Acta. 69 (2012) 247–255. doi:10.1016/j.electacta.2012.02.101.

[17] C. Zhang, H. Duan, J. Zhao, Synergistic inhibition effect of imidazoline derivative and l -cysteine on carbon steel corrosion in a CO_2 -saturated brine solution, Eval. Program Plann. 112 (2016) 160–169. doi:10.1016/j.corsci.2016.07.018.

[18] H. Lgaz, O. Benali, R. Salghi, S. Jodeh, M. Larouj, Pyridinium derivatives as corrosion inhibitors for mild steel in 1M HCl: Electrochemical, surface and quantum chemical studies, Der Pharma Chem. 8 (2016) 172-190. (http://derpharmachemica.com/archive.html)

[19] A. Khadiri, R. Saddik, K. Bekkouche, A. Aouniti, B. Hammouti, N. Benchat, M. Bouachrine, R. Solmaz, Gravimetric, electrochemical and quantum chemical studies of some pyridazine derivatives as corrosion inhibitors for mild steel in 1 M HCl solution, J. Taiwan Inst. Chem. Eng. 58 (2016) 552–564. doi:10.1016/j.jtice.2015.06.031.

[20] M. Lashkari, M.R. Arshadi, DFT studies of pyridine corrosion inhibitors in electrical double layer: Solvent, substrate, and electric field effects, Chem. Phys. 299 (2004) 131–137. doi:10.1016/j.chemphys.2003.12.019.

[21] K.R. Ansari, M.A. Quraishi, A. Singh, S. Ramkumar, I.B. Obote, Corrosion inhibition of N80 steel in 15% HCl by pyrazolone derivatives: Electrochemical, surface and quantum chemical studies, RSC Adv. 6 (2016) 24130–24141. doi:10.1039/c5ra25441h.

[22] R. Ayers, N. Hackerman, Corrosion inhibition in HCl using methyl pyridines, J. Electrochem. Soc. 110 (1963) 507–513. doi:10.1149/1.2425802.

[23] S.A. Abd El-Maksoud, A.S. Fouda, Some pyridine derivatives as corrosion inhibitors for carbon steel in acidic medium, Mater. Chem. Phys. 93 (2005) 84–90. doi:10.1016/j.matchemphys.2005.02.020.

[24] B.G. Ateya , B.E. El-Anadouli and F.M. El-Nizamy, The adsorption of thiourea on mild steel. Corros. Sci. 24 (1984) 509-515. doi:10.1016/0010-938X(84)90033-7.

[25] A.M. Fekry, R.R. Mohamed, Acetyl thiourea chitosan as an eco-friendly inhibitor for mild steel in sulphuric acid medium, Electrochim. Acta. 55 (2010) 1933–1939. doi:10.1016/j.electacta.2009.11.011.

[26] I. Singh, Inhibition of steel corrosion by thiourea derivatives, Corros. 49 (1993) 473–478. doi:10.5006/1.3316074.

[27] M.J. Ondrechen, S. Gozashti, X.M. Wu, M.J. Ondrechen, S. Gozashti, X.M. Wu, An electronic mechanism for electron pairing in antiferromagnetic bridged mixed valence systems An electronic mechanism for electron pairing in antiferromagnetic bridged mixed-valence systems, 3255 (1996). doi:10.1063/1.461970.

[28] S. Ramachandran, B.-L. Tsai, M. Blanco, H. Chen, Y. Tang, W.A. Goddard, Self-assembled monolayer mechanism for corrosion inhibition of iron by imidazolines, Langmuir. 12 (1996) 6419–6428. doi:10.1021/la960646y.

[29] Z. Salarvand, M. Amirnasr, M. Talebian, K. Raeissi, Enhanced corrosion resistance of mild steel in 1 M HCl solution by trace amount of 2-phenyl-benzothiazole derivatives : Experimental , quantum chemical calculations and molecular dynamics (MD) simulation studies, Corros. Sci. 114 (2017) 133–145. doi:10.1016/j.corsci.2016.11.002.

[30] C. Zhang, J. Zhao, Synergistic inhibition effects of octadecylamine and tetradecyl trimethyl ammonium bromide on carbon steel corrosion in the H2S and CO_2 brine solution, Corros. Sci. 126 (2017) 247–254. doi:10.1016/j.corsci.2017.07.006.

[31] V. Jovancicevic, S. Ramachandran, P. Prince, Inhibition of carbon dioxide corrosion of mild steel by imidazolines and their precursors, Corrosion. 55 (1999) 449–455. doi:10.5006/1.3284006.

[32] S.S. Abdel, O.A. Hazzazi, M.A. Amin, K.F. Khaled, On the corrosion inhibition of low carbon steel in concentrated sulphuric acid solutions . Part I : Chemical and electrochemical (AC and DC) studies, Corros. Sci. 50 (2008) 2258–2271. doi:10.1016/j.corsci.2008.06.005.

[33] S.N. Simison, S.R. De Sa, The influence of steel microstructure on CO_2 corrosion . EIS studies on the inhibition efficiency of benzimidazole, Electrochim. Acta. 48 (2003) 845–854. doi:10.1016/S0013-4686(02)00776-4.

[34] K. Jüttner, Electrochemical impedance spectroscopy (EIS) of corrosion processes on inhomogeneous surfaces. Electrochemical Methods in Corrosion Research III, 45 (1989) 191–204. doi:10.4028/www.scientific.net/MSF.44-45.191.

[35] H. Huang, Z. Wang, Y. Gong, F. Gao, Z. Luo, S. Zhang, H. Li, Water soluble corrosion inhibitors for copper in 3.5 wt% sodium chloride solution, Corros. Sci. 123 (2017) 339–350. doi:10.1016/j.corsci.2017.05.009.

[36] H. Tian, W. Li, B. Hou, D. Wang, Insights into corrosion inhibition behavior of multi-active compounds for X65 pipeline steel in acidic oilfield formation water, Corros. Sci. 117 (2017) 43–58. doi:10.1016/j.corsci.2017.01.010.

[37] C. nan Cao, On the impedance plane displays for irreversible electrode reactions based on the stability conditions of the steady-state-II. Two state variables besides electrode potential, Electrochim. Acta. 35 (1990) 837–844. doi:10.1016/0013-4686(90)90078-E.

[38] B. Hirschorn, M.E. Orazem, B. Tribollet, V. Vivier, I. Frateur, M. Musiani, Determination of effective capacitance and film thickness from constant-phase-element parameters, Electrochim. Acta. 55 (2010) 6218–6227. doi:10.1016/j.electacta.2009.10.065.

[39] A. Popova, M. Christov, A. Vasilev, Mono- and dicationic benzothiazolic quaternary ammonium bromides as mild steel corrosion inhibitors . Part III : Influence of the temperature on the inhibition process, Corros. Sci. 94 (2015) 70–78. doi:10.1016/j.corsci.2015.01.039.

[40] J.M. Zhao, H.X. Liu, D.I. Wei, Y. Zuo, The inhibition synergistic effect between imidazoline derivative and thiourea, Electrochemistry. 10 (2004) 440–445. doi:10.13208/j.electrochem.2004.04.013.

[41] G.E. Badr, The role of some thiosemicarbazide derivatives as corrosion inhibitors for C-steel in acidic media, Corros. Sci. 51 (2009) 2529–2536. doi:10.1016/j.corsci.2009.06.017.

[42] I.B. Obot, D.D. Macdonald, Z.M. Gasem, Density functional theory (DFT) as a powerful tool for designing new organic corrosion inhibitors: Part 1: An overview, Corros. Sci. 99 (2015) 1–30. doi:10.1016/j.corsci.2015.01.037.

[43] G.L.F. Mendonça, S.N. Costa, V.N. Freire, P.N.S. Casciano, A.N. Correia, P. de Lima-Neto, Understanding the corrosion inhibition of carbon steel and copper in sulphuric acid medium by amino acids using electrochemical techniques allied to molecular modelling methods, Corros. Sci. 115 (2017) 41–55. doi:10.1016/j.corsci.2016.11.012.

[44] Y. Tang, L. Yao, C. Kong, W. Yang, Y. Chen, Molecular dynamics simulations of dodecylamine adsorption on iron surfaces in aqueous solution, Corros. Sci. 53 (2011) 2046–2049. doi:10.1016/j.corsci.2011.01.051.